

Diffusion synthetic acceleration for heterogeneous domains, compatible with voids

B. S. Southworth^a, Milan Holec^b, T. S. Haut^b

^a *Department of Applied Mathematics, University of Colorado Engineering Center, ECOT 225, 526 UCB, Boulder, CO 80309-0526*

^b *Lawrence Livermore National Laboratory, 7000 East Ave, Livermore, CA 94550.*

*Email: <mailto:ben.s.southworth@gmail.com>

Number of pages: 23

Number of tables: 5

Number of figures: 3

Abstract

A standard approach to solving the S_N transport equations is to use source iteration with diffusion synthetic acceleration (DSA). Although this approach is widely used and effective on many problems, there remain some practical issues with DSA preconditioning, particularly on highly heterogeneous domains. For large-scale parallel simulation, it is critical that both (i) preconditioned source iteration converges rapidly, and (ii) the action of the DSA preconditioner can be applied using fast, scalable solvers, such as algebraic multigrid (AMG). For heterogeneous domains, these two interests can be at odds. In particular, there exist DSA diffusion discretizations that can be solved rapidly using AMG, but they do not always yield robust/fast convergence of the larger source iteration. Conversely, there exist robust DSA discretizations where source iteration converges rapidly on difficult heterogeneous problems, but fast parallel solvers like AMG tend to struggle applying the action of such operators. Moreover, very few current methods for the solution of deterministic transport are compatible with voids. This paper develops a new heterogeneous DSA preconditioner based on only preconditioning the optically thick subdomains. The resulting method proves robust on a wide variety of heterogeneous transport problems, including a linearized hohlraum mesh related to inertial confinement fusion. Moreover, the action of the preconditioner is easily computed using $\mathcal{O}(1)$ AMG iterations, is faster and more robust than current state-of-the-art on all tested problems, and is trivially compatible with voids. On the hohlraum problem, rapid convergence is obtained by preconditioning only 3% of the mesh elements with ≈ 10 AMG iterations.

Keywords — transport, discrete ordinates, high-order, sweep, unstructured

I. INTRODUCTION

Solving the particle transport equations arises in numerous fields of research, such as nuclear reactor design, inertial confinement fusion (ICF), and medical imaging, among others. Despite decades of research, however, it remains a computationally expensive and challenging problem. The simplified steady state, mono-energetic neutral-particle transport equation for the spatially and angularly dependent scalar flux, ψ , is given by

$$\boldsymbol{\Omega} \cdot \nabla \psi(\mathbf{x}, \boldsymbol{\Omega}) + \sigma_t(\mathbf{x})\psi(\mathbf{x}, \boldsymbol{\Omega}) = \frac{\sigma_s(\mathbf{x})}{4\pi} \int_{\mathbb{S}^2} \psi(\mathbf{x}, \boldsymbol{\Omega}') d\boldsymbol{\Omega}' + q_d(\mathbf{x}). \quad (1)$$

Here, $0 \leq \sigma_s \leq \sigma_t$ are the spatially dependent scattering and total cross sections, respectively, and we assume isotropic scattering for simplicity. This equation is fundamental to models of neutral particle transport, such as neutron or photon transport, and also more-or-less a requirement to solve more complicated physical models such as thermal radiative transfer. The left-hand side of (1) is a 3D advection-reaction equation in direction $\boldsymbol{\Omega}$ and the right-hand side an integral-operator coupling over direction. Including time and energy leads to seven dimensions with potentially nonlinear coupling, requiring massively parallel simulations.

In this paper, we consider an S_N angular discretization of the integral operator in (1). Using n directions in the angular quadrature set yields the following semi-discrete form of (1),

$$\begin{aligned} \boldsymbol{\Omega}_d \cdot \nabla_{\mathbf{x}} \psi_d(\mathbf{x}) + \sigma_t(\mathbf{x}) \psi_d(\mathbf{x}) &= q_d(\mathbf{x}) + \frac{\sigma_s(\mathbf{x})}{4\pi} \sum_{d'=1}^n \omega_{d'} \psi_{d'}(\mathbf{x}), \quad \mathbf{x} \in \mathcal{D}, \\ \psi_d(\mathbf{x}) &= \psi_{d,\text{inc}}(\mathbf{x}), \quad \mathbf{x} \in \partial\mathcal{D} \quad \text{and} \quad \mathbf{n}(\mathbf{x}) \cdot \boldsymbol{\Omega}_d < 0, \end{aligned} \quad (2)$$

where subscript d denotes a fixed angle in the S_N angular discretization, with weight ω_d and direction $\boldsymbol{\Omega}_d$. Here $\psi_d(\mathbf{x})$ denotes the angular flux associated with direction d , and the scalar flux is then defined as

$$\varphi(\mathbf{x}) := \sum_{d'=1}^n w_{d'} \psi_{d'}(\mathbf{x}).$$

Due to the high-dimensionality of the transport equations, memory is one of the fundamental constraints in solving them numerically. Fortunately, it is generally the case that $\{\psi_d\}$ can be eliminated from the problem, and the scalar flux φ iterated to convergence, thus only requiring storage of one vector on the spatial domain rather than one for each angle. This is discussed formally in a linear algebraic setting in Section II.B.

A common approach to solve (1) is based on a fixed-point iteration, where each iteration inverts the left-hand side for each direction in the S_N angular discretization. This is referred to as a “transport sweep” and is the dominant computational cost of solving the transport equations. Upwinded discontinuous discretizations are particularly amenable to a sweep (and commonly used for this reason), because the linear system for each direction can be solved directly using a forward solve. A transport sweep then consists of a parallel implementation of simultaneous forward solves for all directions in the quadrature set. For $\sigma_t \ll 1$ or $\sigma_s \ll \sigma_t$, this fixed-point iteration converges rapidly. For $\sigma_t \approx \sigma_s \gg 1$, the fixed-point operator is very slow to converge, but can be effectively preconditioned with so-called diffusion synthetic acceleration (DSA). DSA corresponds to solving an appropriate discrete diffusion operator as a preconditioner for the fixed-point iteration on the scalar flux, which is the focus of this paper.

DSA was developed in separate works in the 1960s as an acceleration technique for solving the transport equations by approximating the behavior of the scalar flux in optically thick materials with a diffusion equation [1, 2]. DSA was analyzed and improved for specific discretizations in the 1970s (for example, [3]) and a new scaling of the transport equations was introduced in [4] to analyze DSA preconditioning. Since, DSA has seen significant research over the years. Some of the most important, general observations include the (i) need for a so-called consistency between the discretization of the linear transport equation and the diffusion

preconditioning, and (ii) the degraded effectiveness of DSA in heterogeneous media [5]. In particular, DSA is known to be effective and easy to apply on homogeneous and optically thick domains, $\sigma_t \gg 1$. However, it is not uncommon for σ_s and σ_t to vary by many orders of magnitude over a spatial domain, and such heterogeneous domains remain difficult for existing methods.

The practical difficulties of DSA on heterogeneous domains comes from trying to satisfy both of the requirements for a fast, parallel transport simulation:

1. The DSA discretization must be an effective preconditioner of the S_N transport equations, resulting in rapid convergence.
2. The DSA preconditioning must be able to be applied in a fast, parallel manner.

These two goals are straightforward to satisfy individually and can both be satisfied for some problems. However, it is often difficult or impossible to satisfy both using existing techniques on highly heterogeneous domains. Part of this problem comes from the requirement of consistency between the transport and diffusion discretizations. In particular, the transport equations are often discretized using some form of upwind discontinuous discretization. It turns out the compatible DSA preconditioner involves inverting a symmetric interior penalty type diffusion discretization. It is well known though that fast solvers such as algebraic multigrid (AMG) tend to struggle on discontinuous discretizations, even of elliptic problems. This is compounded by the fact that these compatible DSA diffusion discretizations can have very poor conditioning in the optically thick limit [6].

Thus the dichotomy is as follows: rapid convergence on highly heterogeneous domains requires DSA based on specific discontinuous diffusion discretizations. However, such discretizations are between difficult and just not amenable to existing fast, parallel linear solvers, such as AMG, particularly if using existing parallel linear solver libraries such as *hypre* [7]. A number of works have considered how to construct more effective algebraic solvers for such diffusion discretizations, including in the transport community [8, 9] as well as the linear solver community [10, 11, 12], but to our knowledge (and experience testing various methods) these discretizations remain difficult for existing methods, particularly methods that are publicly available and implemented in parallel. Furthermore, it is generally the case that DSA bilinear forms have a $1/\sigma_t(\mathbf{x})$ diffusion coefficient, which is not well-defined if there are any regions of vacuum, $\sigma_t = 0$. Some works have developed appropriate linear and nonlinear DSA modifications when using the self-adjoint angular flux formulation of transport [13, 14], but to our knowledge DSA applied to the S_N transport equations in domains with voids remains an open question.

This paper derives a new DSA-like preconditioner (not discretization) for heterogeneous domains, which is (i) easier to apply in a fast and scalable manner with existing solvers than standard DSA, (ii) a better preconditioner than even the most robust standard DSA preconditioners we have tested, and (iii) amenable to vacuum. Conceptually, the new algorithm is quite simple, and more-or-less corresponds to only applying DSA preconditioning on “thick” regions in the domain.^a Using variations in a crooked pipe benchmark problem, the new heterogeneous DSA method reduces the total number of iterations to convergence by 5 – 6× for some problems. Moreover, the heterogeneous DSA matrices are more tractable to solve using AMG, in a number of tests converging in $\mathcal{O}(1)$ iterations when AMG was unable to solve the full DSA matrix. The new method is relatively non-intrusive, in the sense that it can be added to existing libraries that support DSA with minimal work. Conceptually, the preconditioner is independent of the discretization. However, a discussion on implementation and numerical results are presented based on a discontinuous Galerkin (DG) discretization of the S_N transport equations and corresponding DG DSA discretization [6, 16].

Section II presents standard source iteration and DSA in the context of block preconditioners. This motivates a similar analysis applied specifically to DSA preconditioning, and

^aRecent work in [15] has seen success applying similar ideas to precondition the radiation diffusion equations by only solving the diffusion discretization on a physical subdomain.

the development of the new heterogeneous DSA preconditioning in Section II.C. An implementation involving the *hypr*e library and DG spatial discretizations is discussed in Section III, including a generalization of the modified penalty coefficient introduced in [16] for high-order curvilinear meshes. Numerical results then demonstrate the new method on heterogeneous domains in Section IV, including on variations of a crooked pipe problem [17, 18], and a linearized hohlraum capsule. For the hohlraum, in particular, rapid convergence is obtained when applying (heterogeneous) DSA preconditioning to $\approx 3\%$ of mesh elements! Some conclusions are given in Section V.

II. PRECONDITIONING LINEAR TRANSPORT

II.A. Review of 2×2 block preconditioners

Source iteration and diffusion synthetic acceleration (DSA) applied to linear S_N transport can be seen in a linear-algebraic framework as a block preconditioning of a 2×2 block operator. A linear-algebraic perspective on transport iterations was introduced as early as 1989 in [19]^b, and transport iterations are often expressed in algebraic operator form (for example, see [16]). The specific context of 2×2 block preconditioners is not something seen often in the literature, but provides valuable insight on the preconditioning of heterogeneous domains.

As background, consider a 2×2 block matrix A and lower-triangular preconditioner L ,

$$A = \begin{bmatrix} A_{11} & A_{12} \\ A_{21} & A_{22} \end{bmatrix}, \quad L = \begin{bmatrix} A_{11} & \mathbf{0} \\ A_{21} & \widehat{\mathcal{S}} \end{bmatrix}, \quad (3)$$

where $\mathcal{S} := A_{22} - A_{21}A_{11}^{-1}A_{12}$ is the Schur complement of A in the $(2,2)$ -block, and $\widehat{\mathcal{S}}$ some approximation to \mathcal{S} . In the simplest case of a block Gauss-Seidel like iteration, we have $\widehat{\mathcal{S}} := A_{22}$. It can be shown that fixed-point or Krylov iterations applied to $A\mathbf{x} = \mathbf{b}$ with preconditioner L^{-1} converge to some tolerance $< C\epsilon$ after k iterations if and only if equivalent iterations applied to a Schur complement problem $\mathcal{S}\mathbf{x}_c = \mathbf{b}_c$, with preconditioner $\widehat{\mathcal{S}}^{-1}$, converge to tolerance ϵ after k iterations, where $C \sim \mathcal{O}(\|A_{11}^{-1}A_{12}\|)$ [20]. As it turns out, source iteration and DSA preconditioning correspond exactly to a block lower-triangular preconditioning, as in (3), and considering transport iterations in the context of block preconditioners allows us to derive a natural approach to DSA preconditioning in heterogeneous media.

II.B. Source iteration as a block preconditioner

Now suppose the left-hand side of (2) is discretized in space for each direction d , with corresponding discrete spatial operator $\mathcal{L}_d \sim \boldsymbol{\Omega}_d \cdot \nabla_{\mathbf{x}} + \sigma_t$, and let Σ_s and Σ_t denote mass matrices with respect to coefficients $\sigma_s(\mathbf{x})/4\pi$ and $\sigma_t(\mathbf{x})$, respectively. Further, let bold $\boldsymbol{\psi}_d$ and \mathbf{q}_d denote the discrete vector representations of $\psi_d(\mathbf{x})$ and $q_d(\mathbf{x})$. Then, the full discretized set of equations can be written as a block linear system,

$$\begin{bmatrix} \mathcal{L}_1 & & & & -\Sigma_s \\ & \ddots & & & \vdots \\ & & \mathcal{L}_n & & -\Sigma_s \\ \text{-----} & & & & I \\ -\omega_1 I & \dots & -\omega_n I & & \end{bmatrix} \begin{bmatrix} \boldsymbol{\psi}_1 \\ \vdots \\ \boldsymbol{\psi}_n \\ \boldsymbol{\varphi} \end{bmatrix} = \begin{bmatrix} \mathbf{q}_1 \\ \vdots \\ \mathbf{q}_n \\ \mathbf{0} \end{bmatrix}. \quad (4)$$

The dotted lines indicate how the S_N transport equations can be expressed as a 2×2 block array (3): A_{11} is the block-diagonal set of spatial operators, $\{\mathcal{L}_d\}$, $A_{22} = I$, and the off-diagonal operators A_{12} and A_{21} correspond to scattering and quadrature weights, respectively.

^bUnfortunately, the only available copy of [19] appears to be a low-resolution, scanned in copy, which is difficult to read.

One of the standard approaches to solve (4) in transport simulations is to update the scalar flux based on the current angular flux,

$$\boldsymbol{\psi}_d^{(i+1)} = \mathcal{L}_d^{-1}(\mathbf{q}_d + \Sigma_s \boldsymbol{\varphi}^{(i)}), \quad (5)$$

for all directions $d = 1, \dots, n$. With updated scalar flux for each direction, the angular flux is then updated by summing the scalar flux over quadrature weights $\{\omega_d\}$,

$$\boldsymbol{\varphi}^{(i+1)} = \sum_{d=1}^n \omega_d \boldsymbol{\psi}_d^{(i+1)} = \sum_{d=1}^n \omega_d \mathcal{L}_d^{-1} \left(\mathbf{q}_d + \Sigma_s \boldsymbol{\varphi}^{(i)} \right). \quad (6)$$

This process is repeated and is the classical ‘‘source iteration.’’ Algebraically, source iteration is exactly a fixed-point iteration with block lower-triangular preconditioning:

$$\begin{bmatrix} \boldsymbol{\psi}_1^{(i+1)} \\ \vdots \\ \boldsymbol{\psi}_n^{(i+1)} \\ \boldsymbol{\varphi}^{(i+1)} \end{bmatrix} = \begin{bmatrix} \boldsymbol{\psi}_1^{(i)} \\ \vdots \\ \boldsymbol{\psi}_n^{(i)} \\ \boldsymbol{\varphi}^{(i)} \end{bmatrix} + \begin{bmatrix} \mathcal{L}_1 & & & \\ & \ddots & & \\ & & \mathcal{L}_n & \\ -\omega_1 I & \dots & -\omega_n I & I \end{bmatrix}^{-1} \left(\begin{bmatrix} \mathbf{q}_1 \\ \vdots \\ \mathbf{q}_n \\ \mathbf{0} \end{bmatrix} - \begin{bmatrix} \mathcal{L}_1 & & & -\Sigma_s \\ & \ddots & & \vdots \\ & & \mathcal{L}_n & -\Sigma_s \\ -\omega_1 I & \dots & -\omega_n I & I \end{bmatrix} \begin{bmatrix} \boldsymbol{\psi}_1^{(i)} \\ \vdots \\ \boldsymbol{\psi}_n^{(i)} \\ \boldsymbol{\varphi}^{(i)} \end{bmatrix} \right).$$

Expanding, one arrives at exactly the two stage iteration for $\{\boldsymbol{\psi}_d\}$ and $\boldsymbol{\varphi}$ introduced in (5) and (6). In this form, it is also clear how Krylov methods can be applied to accelerate convergence of source iteration [21, 5]. In particular, Krylov methods require computing the action of the operator, A , and preconditioner, M^{-1} , on vectors, where

$$A = \begin{bmatrix} \mathcal{L}_1 & & & -\Sigma_s \\ & \ddots & & \vdots \\ & & \mathcal{L}_n & -\Sigma_s \\ -\omega_1 I & \dots & -\omega_n I & I \end{bmatrix}, \quad M^{-1} = \begin{bmatrix} \mathcal{L}_1^{-1} & & & \\ & \ddots & & \\ & & \mathcal{L}_n^{-1} & \\ \omega_1 \mathcal{L}_1^{-1} & \dots & \omega_n \mathcal{L}_n^{-1} & I \end{bmatrix}.$$

Note that in source iteration, the so-called transport sweep inverts \mathcal{L}_d^{-1} for all $d = 1, \dots, n$, meaning that in the 2×2 block sense, A_{11} is inverted exactly. Recall from Section II.A that convergence of fixed-point or Krylov iterations with a 2×2 block lower-triangular preconditioner are then defined by equivalent iterations on the preconditioned Schur complement problem. In this case, in the notation of (3), we have $\hat{S} = A_{22} = I$, and the preconditioned Schur complement takes the form $\mathcal{S}\boldsymbol{\varphi} = \mathbf{b}$, where

$$\mathcal{S} := I - \begin{bmatrix} \omega_1 I & \dots & \omega_n I \end{bmatrix} \begin{bmatrix} \mathcal{L}_1^{-1} & & \\ & \ddots & \\ & & \mathcal{L}_n^{-1} \end{bmatrix} \begin{bmatrix} \Sigma_s \\ \vdots \\ \Sigma_s \end{bmatrix} = I - \sum_{d=1}^n \omega_d \mathcal{L}_d^{-1} \Sigma_s, \quad (7)$$

and $\mathbf{b} := \sum_{d=1}^n \omega_d \mathcal{L}_d^{-1} \mathbf{q}_d$. If \mathcal{S} is well conditioned, such as in the optically thin case when $\Sigma_s \ll 1$, we can solve $-\mathcal{S}\boldsymbol{\varphi} = \mathbf{b}$ via a simple Richardson iteration,

$$\boldsymbol{\varphi}^{(i+1)} = \boldsymbol{\varphi}^{(i)} + \mathbf{b} + \mathcal{S}\boldsymbol{\varphi}^{(i)} = \sum_{d=1}^n \omega_d \mathcal{L}_d^{-1} \left(\mathbf{q}_d + \Sigma_s \boldsymbol{\varphi}^{(i)} \right). \quad (8)$$

If \mathcal{S} is ill conditioned, such as in optically thick or heterogeneous media, some form of preconditioner for \mathcal{S} is necessary for fast convergence. In the larger system, this simply replaces the I in the lower right (2, 2)-block of the preconditioner, M^{-1} , with some approximation to

\mathcal{S} . Denoting this approximation \mathcal{D} , the preconditioner takes the form

$$M^{-1} = \begin{bmatrix} \mathcal{L}_1 & & & \\ & \ddots & & \\ & & \mathcal{L}_n & \\ -\omega_1 I & \dots & -\omega_n I & \mathcal{D} \end{bmatrix}^{-1} = \begin{bmatrix} I & & & \\ & \ddots & & \\ & & I & \\ & & & \mathcal{D}^{-1} \end{bmatrix} \begin{bmatrix} \mathcal{L}_1^{-1} & & & \\ & \ddots & & \\ & & \mathcal{L}_n^{-1} & \\ \omega_1 \mathcal{L}_1^{-1} & \dots & \omega_n \mathcal{L}_n^{-1} & I \end{bmatrix}. \quad (9)$$

Now, convergence of fixed-point or Krylov iterations applied to the larger system (4) is equivalent to convergence of iterations applied to $\mathcal{D}^{-1}\mathcal{S}$. In assuming that \mathcal{L}_d is inverted for all d (rather than, say, an on-processor solve), $\{\psi_d\}$ can be eliminated from the system, yielding a preconditioned fixed-point iteration on φ ,

$$\varphi^{(i+1)} = \varphi^{(i)} + \mathcal{D}^{-1} \left(\varphi^{(i)} - \sum_{d=1}^n \omega_d \mathcal{L}_d^{-1} (\Sigma_s \varphi^{(i)} + \mathbf{q}_d) \right). \quad (10)$$

At any point, an approximation to the angular flux can be computed via equation (5) (and is implicitly computed within every iteration). Similar to the case of source iteration, it is straightforward to analyze and implement Krylov methods here as well, where \mathcal{S} is the operator and \mathcal{D}^{-1} the preconditioner. It is worth pointing out that for linear S_N transport as considered here, if angular flux $\{\psi_d^{(i+1)}\}$ is eliminated from the system, it is clear that Krylov convergence is defined by convergence on the Schur complement (scalar flux). For nonlinear or time-dependent transport problems, where the angular flux cannot be fully eliminated, this relation is less obvious without considering iterations in the context of 2×2 block-preconditioning and appealing to the theory on block preconditioners and Krylov methods [20].

Note that in practice, \mathcal{D} is not directly a diffusion operator, rather $\mathcal{D}^{-1} = I + D^{-1}$ is an additive preconditioner, with diffusion operator D . There are various ways to motivate the additive preconditioner. Conceptually, a diffusion operator can be derived in which $D^{-1}\mathcal{S}$ is well-conditioned in the optically thick limit of mean free path $\varepsilon \ll 1$ (for DG discretizations, see [16, 6]). However, in optically thin material, $\Sigma_s \ll 1$, $D^{-1}\mathcal{S}$ can be ill conditioned because \mathcal{S} is already well conditioned in thin material, but the spectrum of D^{-1} goes to zero for high-frequency modes. Adding the identity shifts such eigenmodes so that $(I + D^{-1})\mathcal{S}$ is well conditioned in thin regimes, while for thick, note that if $D^{-1}\mathcal{S}$ is positive and well-conditioned, then $(I + D^{-1})\mathcal{S}$ is also positive and well-conditioned.

Remark 1. *If \mathcal{L}_d is not inverted exactly due to, for example, block Jacobi iterations instead of a sweep or cycle-breaking on high-order curvilinear meshes [22], it is straightforward to work out a reduced iteration similar to above, which stores φ and the degrees-of-freedom (DOFs) of ψ_d necessary to update each direction d . Extending this to the Krylov setting takes a little more care, but follows in an analogous manner [23].*

II.C. Heterogeneous DSA with two regions

Now consider the case of heterogeneous domains, and suppose we partition the domain into “thin” and “thick” regions. In particular, let DOFs/elements in which $\sigma_s(\mathbf{x}) < \eta$ be considered thin, denoted by subscript s , and DOFs/elements such that $\sigma_s(\mathbf{x}) \geq \eta$ be considered thick, denoted with subscript f . Then, order all matrices $\{\mathcal{L}_d\}$ in a block ordering

$$\mathcal{L}_d = \begin{bmatrix} L_{ss} & L_{sf} \\ L_{fs} & L_{ff} \end{bmatrix}.$$

Note that these region do not have to be contiguous. Moving forward, subscripts d denoting angle are dropped on submatrices L_{ss}, L_{sf}, L_{fs} , and L_{ff} , for ease of notation. Note, however, that summations over direction d have an implied subscript on submatrices of \mathcal{L}_d .

Now, recall the two Schur complements of \mathcal{L}_d ,

$$\mathcal{S}_{ss} = L_{ss} - L_{sf}L_{ff}^{-1}L_{fs}, \quad \mathcal{S}_{ff} = L_{ff} - L_{fs}L_{ss}^{-1}L_{sf}, \quad (11)$$

and the closed form inverse of a 2×2 block matrix (see, for example, [24, 3.2.11]),

$$\mathcal{L}_d^{-1} = \begin{bmatrix} \mathcal{S}_{ss}^{-1} & -L_{ss}^{-1}L_{sf}\mathcal{S}_{ff}^{-1} \\ -\mathcal{S}_{ff}^{-1}L_{fs}L_{ss}^{-1} & \mathcal{S}_{ff}^{-1} \end{bmatrix}, \quad (12)$$

where

$$\mathcal{S}_{ss}^{-1} = L_{ss}^{-1} + L_{ss}^{-1}L_{sf}\mathcal{S}_{ff}^{-1}L_{fs}L_{ss}^{-1}, \quad \mathcal{S}_{ff}^{-1} = L_{ff}^{-1} + L_{ff}^{-1}L_{fs}\mathcal{S}_{ss}^{-1}L_{sf}L_{ff}^{-1}$$

are interdependent expressions for the inverse of a Schur complement. Using (12), we can expand the Schur complement (7) in block form as

$$\begin{aligned} \mathcal{S} &= I - \sum_{d=1}^n \omega_d \mathcal{L}_d^{-1} \Sigma_s \\ &= I - \sum_{d=1}^n \omega_d \begin{bmatrix} \mathcal{S}_{ss}^{-1} & -L_{ss}^{-1}L_{sf}\mathcal{S}_{ff}^{-1} \\ -\mathcal{S}_{ff}^{-1}L_{fs}L_{ss}^{-1} & \mathcal{S}_{ff}^{-1} \end{bmatrix} \begin{bmatrix} \Sigma_{s,s} \\ \Sigma_{s,f} \end{bmatrix}. \end{aligned} \quad (13)$$

Observe that Σ_s is a column scaling. Suppose the thin region is actually vacuum, in which case $\Sigma_{s,s} = \mathbf{0}$. Then,

$$\begin{aligned} \mathcal{S} &= I - \sum_{d=1}^n \omega_d \begin{bmatrix} \mathbf{0} & -L_{ss}^{-1}L_{sf}\mathcal{S}_{ff}^{-1}\Sigma_{s,f} \\ \mathbf{0} & \mathcal{S}_{ff}^{-1}\Sigma_{s,f} \end{bmatrix} \\ &= \begin{bmatrix} I & \sum_{d=1}^n \omega_d L_{ss}^{-1}L_{sf}\mathcal{S}_{ff}^{-1}\Sigma_{s,f} \\ \mathbf{0} & I - \sum_{d=1}^n \omega_d \mathcal{S}_{ff}^{-1}\Sigma_{s,f} \end{bmatrix}. \end{aligned} \quad (14)$$

Looking at (14), a natural choice of preconditioner for \mathcal{S} is a block upper-triangular preconditioner, with ‘‘blocks’’ indicating thin and thick regions of the domain. Now we only need to precondition the lower right (thick) block of (14), $I - \sum_{d=1}^n \omega_d \mathcal{S}_{ff}^{-1}\Sigma_{s,f}$. A natural choice here is to approximate \mathcal{S}_{ff}^{-1} in the lower diagonal block (but not in the off-diagonal block) by L_{ff}^{-1} , in some sense a first-order approximation from (11). This yields,

$$\mathcal{S} \approx \begin{bmatrix} I & \sum_{d=1}^n \omega_d L_{ss}^{-1}L_{sf}\mathcal{S}_{ff}^{-1}\Sigma_{s,f} \\ \mathbf{0} & I - \sum_{d=1}^n \omega_d L_{ff}^{-1}\Sigma_{s,f} \end{bmatrix}. \quad (15)$$

Now, disregarding boundary conditions, $I - \sum_{d=1}^n \omega_d L_{ff}^{-1}\Sigma_{s,f}$ corresponds to S_N transport only on the thick region, for which we know that diffusion is an effective preconditioning. Letting D_{ff}^{-1} denote an appropriate diffusion discretization over the thick region, we use the preconditioner $I + D_{ff}^{-1} \approx (I - \sum_{d=1}^n \omega_d L_{ff}^{-1}\Sigma_{s,f})^{-1} \approx (I - \sum_{d=1}^n \omega_d \mathcal{S}_{ff}^{-1}\Sigma_{s,f})^{-1}$, which can be applied as the first step in a block upper triangular preconditioning,

$$\begin{aligned} \mathcal{D}_T^{-1} &= \begin{bmatrix} I & \sum_{d=1}^n \omega_d L_{ss}^{-1}L_{sf}\mathcal{S}_{ff}^{-1}\Sigma_{s,f} \\ \mathbf{0} & (I + D_{ff}^{-1})^{-1} \end{bmatrix}^{-1} \\ &= \begin{bmatrix} I & -\sum_{d=1}^n \omega_d L_{ss}^{-1}L_{sf}\mathcal{S}_{ff}^{-1}\Sigma_{s,f} \\ \mathbf{0} & I \end{bmatrix} \begin{bmatrix} I & \mathbf{0} \\ \mathbf{0} & I + D_{ff}^{-1} \end{bmatrix}. \end{aligned} \quad (16)$$

The resulting preconditioning corresponds to a DSA preconditioning only on the thick region

(including interface), followed by using the updated thick solution as an additive correction to the thin region. Note that applying DSA only on the thick region is *not* the same as inverting a global diffusion operator and only updating the thick DOFs.

To apply the additive correction in the left block of (16), following DSA on the thick region, note from (12) that

$$\begin{bmatrix} I & -\sum_{d=1}^n \omega_d L_{ss}^{-1} L_{sf} \mathcal{S}_{ff}^{-1} \Sigma_{s,f} \\ \mathbf{0} & I \end{bmatrix} = I + \begin{bmatrix} I & \mathbf{0} \\ \mathbf{0} & \mathbf{0} \end{bmatrix} \sum_{d=1}^n \omega_d \mathcal{L}_d^{-1} \Sigma_s \begin{bmatrix} \mathbf{0} & \mathbf{0} \\ \mathbf{0} & I \end{bmatrix}.$$

This is nothing more than a modified transport sweep with zero right-hand side. For all angles, the angular flux is first set to zero on the thin region, then a transport sweep is applied, inverting \mathcal{L}_d for each direction d , but only accumulating the solution corrections in thin DOFs. The action of the preconditioner (16) can be expressed as two steps:

Algorithm 1 (Triangular heterogeneous DSA).

1. Let φ_f denote φ restricted to the thick region, and update $\varphi_f \leftarrow \varphi_f + D_{ff}^{-1} \varphi_f$, where D_{ff} is a DSA diffusion preconditioner over the thick region.
2. Define $\bar{\varphi} := \begin{bmatrix} \mathbf{0} \\ \varphi_f \end{bmatrix}$, and let φ_s denote φ restricted to the thin region. For each direction d , update φ_s via

$$\varphi_s \leftarrow \varphi_s + [\omega_d \mathcal{L}_d^{-1} \Sigma_s \bar{\varphi}]_s.$$

In the case of $\Sigma_{s,s} = \mathbf{0}$, \mathcal{S} is indeed block upper triangular, and the convergence of block-triangular preconditioned minimal-residual methods is defined by the approximation of the (2,2)-block in \mathcal{S} . For $\Sigma_{s,s} > 0$, \mathcal{S} is no longer triangular, and convergence is then defined by preconditioning of the (2,2)-Schur complement of \mathcal{S} [20]. However, when $\Sigma_{s,s}$ is small, this preconditioning will likely be comparable to the preconditioning of the (2,2)-block in \mathcal{S} , analogous to when $\Sigma_{s,s} = \mathbf{0}$. That is, convergence of heterogeneous-DSA-preconditioned source iteration is expected to be comparable for general $\Sigma_{s,s} \ll 1$, which is consistent with numerical results in Section IV.

In many cases block-triangular preconditioners offer faster convergence than block-diagonal, with marginal additional cost. For heterogeneous DSA, however, computing the action of the off-diagonal blocks requires a full parallel sweep. Thus, a second option for heterogeneous DSA preconditioning is a block-diagonal preconditioner, eliminating the need for the additional sweep in Algorithm 1. Define the preconditioner

$$\mathcal{D}_D^{-1} = \begin{bmatrix} I & \mathbf{0} \\ \mathbf{0} & I + D_{ff}^{-1} \end{bmatrix}. \quad (17)$$

for which the action can be described as follows.

Algorithm 2 (Diagonal heterogeneous DSA).

1. Let φ_f denote φ restricted to the thick region, and update $\varphi_f \leftarrow \varphi_f + D_{ff}^{-1} \varphi_f$, where D_{ff} is the DSA diffusion preconditioner over the thick region.

When preconditioning by inverting the diagonal blocks of a 2×2 operator, block-diagonal preconditioned minimal-residual iterations generally converge to a given tolerance in roughly twice as many iterations as block-triangular preconditioners, due to not capturing off-diagonal coupling in the preconditioner [20]. For more general approximations (as used here), the difference in convergence between block-diagonal and block-triangular preconditioning is more complicated. In particular, there are situations where block-diagonal preconditioning can converge as fast as block-triangular, or many times slower [25]. In almost all problems we have

tested, heterogeneous DSA appears to fall into the former – block-diagonal preconditioning results in convergence as good as, or almost as good as, block-triangular preconditioning, at a fraction of the cost. Block-triangular preconditioning has resulted in fewer iterations on a few problems where $\Sigma_{s,s} \sim \mathcal{O}(1)$ is considered “thin” (for example, see Figure 2), but due to the auxiliary sweep, the overall time-to-solution remained longer than with block-diagonal preconditioning. Block-diagonal preconditioning has the additional advantage over block-triangular preconditioning that it can be used with conjugate gradient or MINRES if the scalar flux problem is symmetrized, as in [26, 27].

Thus, the main algorithm proposed here is very simple: only apply DSA preconditioning on the thick region. It is immediately apparent why this is also compatible with voids, because if $\Sigma_t = \mathbf{0}$ on a certain region in the problem domain, a diffusion approximation (typically depending on Σ_t^{-1}) is neither formed nor inverted on that region. It is important to note that heterogeneous DSA is *not the same* as inverting a global DSA preconditioner and only applying updates to the thin region.

Remark 2 (Block-diagonal vs. block-triangular heterogeneous DSA). *Examples were constructed in [25] where block-diagonal preconditioned minimal-residual iterations took up to 10× more iterations to converge than with block-triangular preconditioning. If such a problem were to arise in transport, the auxiliary sweep in block-triangular heterogeneous DSA would likely be worth the added computational cost. Moreover, block-diagonal preconditioners typically rely more heavily on Krylov acceleration for convergence. When preconditioning source iteration without Krylov acceleration, block-triangular preconditioning likely provides a more robust method.*

III. IMPLEMENTATION

III.A. DSA discretizations

Conceptually, the heterogeneous preconditioning technique developed in Section II is flexible in terms of underlying transport and diffusion discretization. This paper focuses on discontinuous Galerkin (DG) discretizations of the spatial transport equation and thus, for consistency, DG DSA discretizations as well. DG is of particular interest because the discontinuous finite-element framework is amenable to traditional techniques such as sweeping, and allows for high-order accuracy, including discretizing on high-order curvilinear finite elements.

DSA preconditioning for DG discretizations of S_N transport has been considered in a number of papers, perhaps originally in [8] and more recently considering high-order discretizations in [6, 16]. Here, we build our DSA discretization based on the discrete analysis performed in [6], and extending modified stabilization ideas from [16]. Following the standard derivation of DG discretization, the S_N transport equations in the diffusive-limit scaling [4] can be written in the discrete form

$$\boldsymbol{\Omega}_d \cdot \mathbf{G} \boldsymbol{\psi}^{(d)} + F^{(d)} \boldsymbol{\psi}^{(d)} + \frac{1}{\varepsilon} \Sigma_t \boldsymbol{\psi}^{(d)} - \frac{1}{4\pi} \left(\frac{1}{\varepsilon} \Sigma_t - \varepsilon \Sigma_a \right) \boldsymbol{\varphi} = \frac{1}{4\pi} \left(\mathbf{q}_{\text{inc}}^{(d)} + \varepsilon \mathbf{q}^{(d)} \right). \quad (18)$$

where ε is the characteristic mean-free path, $\boldsymbol{\psi}_d$ is the angular flux vector for the d th discrete ordinate direction, and $\boldsymbol{\varphi}$ is the scalar flux, given by

$$\boldsymbol{\varphi} = \sum_d \omega_d \boldsymbol{\psi}^{(d)},$$

for quadrature weights $\{\omega_d\}$. Here Σ_a , Σ_s , and Σ_t are mass matrices corresponding to coefficients $\sigma_a(\mathbf{x})$, $\sigma_s(\mathbf{x})$, and $\sigma_t(\mathbf{x})$, respectively; $F^{(d)}$ is the DG face matrix based on upwinding with respect to $\boldsymbol{\Omega}_d$; and $\boldsymbol{\Omega}_d \cdot \mathbf{G}$ is the element-wise discretization of advection in direction $\boldsymbol{\Omega}_d$. For more details, see [6].

The analysis in [6] proves that a symmetric interior penalty (SIP) discretization provides

a robust DSA preconditioner in the optically thick limit, $\varepsilon \ll 1$, given by

$$D_{\text{SIP}} = \frac{1}{\varepsilon} F_0 + \frac{1}{3} \mathbf{G}^T \cdot \Sigma_t^{-1} \mathbf{G} - \tilde{\mathbf{F}}_1 \cdot \Sigma_t^{-1} \mathbf{G} + \mathbf{G}^T \cdot \Sigma_t^{-1} \mathbf{F}_1 + \Sigma_a, \quad (19)$$

where

$$F_0 = \frac{1}{4\pi} \sum_d w_d F^{(d)}, \quad \mathbf{F}_1 = \frac{1}{4\pi} \sum_d w_d \boldsymbol{\Omega}_d F^{(d)}, \quad \tilde{\mathbf{F}}_1 = \frac{1}{4\pi} \sum_d w_d \boldsymbol{\Omega}_d \tilde{F}^{(d)},$$

and $\tilde{F}^{(d)}$ corresponds to the bilinear form

$$\mathbf{v}^T \tilde{F}^{(d)} \mathbf{u} = - \sum_{\Gamma \in \mathcal{F}} \int_{\Gamma} \boldsymbol{\Omega}_d \cdot \mathbf{n} \{u\} \llbracket v \rrbracket dS + \sum_{\Gamma \in \mathcal{F}} \int_{\Gamma} \frac{1}{2} |\boldsymbol{\Omega}_d \cdot \mathbf{n}| \llbracket u \rrbracket \llbracket v \rrbracket dS,$$

which satisfies $\boldsymbol{\Omega}_d \cdot \mathbf{G} + F^{(d)} = -\boldsymbol{\Omega}_d \cdot \mathbf{G}^T + \tilde{F}^{(d)}$ [6].

Numerical results in [6] then indicate that dropping the face term $\mathbf{G}^T \cdot \Sigma_t^{-1} \mathbf{F}_1$, leading to a nonsymmetric interior penalty (NIP) discretization, provides a more robust preconditioner in non-optically thick material,

$$D_{\text{NIP}} = \frac{1}{\varepsilon} F_0 + \frac{1}{3} \mathbf{G}^T \cdot \Sigma_t^{-1} \mathbf{G} - \tilde{\mathbf{F}}_1 \cdot \Sigma_t^{-1} \mathbf{G} + \Sigma_a. \quad (20)$$

For linear DG discretizations and straight-edged meshes, D_{NIP} is analogous to the Warsa-Wareing-Morel consistent diffusion discretization developed in [28]. Moreover, with some work, one can show that D_{NIP} can also be derived by integrating the first two angular moments of (2). We use D_{NIP} as our baseline DSA discretization here, as we have found it to be far more robust on heterogeneous domains than D_{SIP} .

III.A.1. Modified penalty coefficient

The interior penalty term F_0 properly enforces continuity of the solution in (19) and (20) in the optically thick limit, $\varepsilon \ll 1$. However, the penalizing term scales as $\frac{1}{\varepsilon} F_0$ and tends to zero in the optically thin limit, $\varepsilon \gg 1$, and the preconditioners (19) and (20) are found to be unstable. In particular, by continuity of eigenvalues as a function of matrix entries, as $\varepsilon \rightarrow 0$, (19) transitions continuously from being SPD to being an indefinite operator. This can lead to eigenvalues very close to zero, which are very difficult to precondition. We introduce the following modified penalizing term,

$$\tilde{F}_0 = \frac{1}{8\pi} \sum_d w_d \sum_{\Gamma} \int_{\Gamma} \max \left(\frac{c(p^{up})}{\sigma_t^{up} h^{up}}, 1 \right) |\boldsymbol{\Omega}_d \cdot \mathbf{n}| \llbracket u \rrbracket \llbracket v \rrbracket dS. \quad (21)$$

Here, the sum is over mesh faces Γ , \mathbf{n} is the normal vector to the face Γ , h is the cell size, $c(p) = Cp(p+1)$ for constant C (we use $C = 0.1$ via testing for the fastest convergence), p is the polynomial order of test and trial functions v and u , and $\llbracket \cdot \rrbracket$ is the jump operator. The label up represents the value on the upwind side at the integration point of the face Γ with respect to direction $\boldsymbol{\Omega}_d$. Note, that (21) coincides with the modified interior penalty formulation in [16], but it introduces a general formulation valid on curvilinear meshes, where the upwind value can vary along a highly curved face. The modified form of the penalty term (21) cancels the scaling ε^{-1} in the thin limit of (19) and (20) and the penalization successfully enforces the continuity for any transport regime. mNIP is used to denote the resulting modified nonsymmetric interior penalty discretization.

III.B. Heterogeneous DSA implementation

Implementing heterogeneous DSA requires identifying and discretizing on a “thick” subdomain. In doing so, we want (i) the method to be amenable to easy addition to existing codes, (ii) the DSA discretization to be an effective preconditioning on the thick subdomain, and (iii)

the DSA discretization on the subdomain to be solvable using standard AMG techniques.

Building on these ideas, we first define a tolerance, η , where mesh elements such that $\sigma_s(\mathbf{x}) \geq \eta$ are considered thick and mesh elements such that $\sigma_s(\mathbf{x}) < \eta$ are considered thin. On every processor, it is straightforward to evaluate σ_s on each mesh element and track which elements are considered thick and thin. Next, suppose we discretize a global DSA operator (as if we are doing normal “full” DSA) and then extract the principle submatrix corresponding to thick DOFs. The resulting matrix represents the thick region throughout the interior of the subdomain, with weakly enforced Dirichlet boundary conditions. The only point that requires additional attention is that face matrices of thick subdomain boundary elements (that is, interior elements of the global mesh at the interface between thick and thin regions) include an interface coupling of σ_t in the thick *and* thin regions (see $\tilde{\mathbf{F}}_1 \cdot \Sigma_t^{-1} \mathbf{G}$ in (20)). Even on the boundary, strong heterogeneities and $\sigma_t \ll 1$ can cause difficulties for AMG. We propose three methods of handling the thick subdomain boundary:

1. Extract directly from the full DSA matrix (that is, do not modify σ_t on thick subdomain boundaries).
2. On thick subdomain boundaries, extend values of σ_t from the thick region to neighboring thin elements. The result is a DSA discretization on the subdomain with no representation of the interface in σ_t . Denote this approach with a *b*-subscript, e.g., NIP_{*b*}.
3. For thin elements neighboring a thick subdomain, let $\sigma_t := \max\{C_\sigma, \sigma_t(\text{el})\}$, where $\sigma_t(\text{el})$ is σ_t evaluated in the thin element and C_σ some minimum value of σ_t . The result is a DSA discretization on the subdomain with a partial representation of the interface in σ_t . Denote this approach as a function of C_σ , e.g., NIP(10) for $C_\sigma = 10$.

The first option is likely the most efficient from a preconditioning perspective, but in some (not all) cases is difficult for linear solvers due to the boundary interface. Ignoring the σ_t -interface in the subdomain discretization has the opposite effect – it is the easiest from a linear solver perspective, but we identified one example where the quality of preconditioning degraded significantly compared with the first option (see Table II in Section IV.A.2), meaning ignoring the interface altogether is not robust as a preconditioner. The third option is a middle-ground between the first two. Although it adds a new free parameter to tune, all numerical results have indicated it to be as effective of a preconditioner as the first option, with comparable AMG performance to the second.

From an implementation perspective, forming the subdomain discretization in each of the above cases requires at most a slightly modified σ_t coefficient and the extraction of the submatrix corresponding to thick DOFs. The *hypre* library [7] now supports parallel extraction of submatrices from a parallel *hypre* matrix, given a (local) list of row/column-indices. *hypre* is one of the standard parallel multigrid libraries and, if not already being used for linear solves in a software package, is easily connected to facilitate this operation.^c

IV. NUMERICAL RESULTS

This section demonstrates the efficacy of the heterogeneous DSA approach on difficult problems in transport with heterogeneous cross sections. We emphasize both the superior and more robust preconditioning that heterogeneous DSA offers over traditional “full” DSA, as well as the important property that the resulting linear systems are more tractable to solve, typically with $\mathcal{O}(1)$ AMG iterations, independent of problem size.

AMG solves are performed using BoomerAMG in the *hypre* library [7]. It is well-known that the choice of parameters is important for AMG. Here we use a V(1, 1)-cycle with ℓ^1 hybrid Gauss-Seidel relaxation (*hypre* type 8) [29], extended+*i* (distance-two) interpolation (*hypre*

^cNote, for an optimized implementation, it is likely preferable to only discretize and construct the DSA matrix on the thick subdomain, particularly if the thick region is very small (for example, see Section IV.B). However, for many finite-element libraries or existing code bases, this ends up being more intrusive to implement.

type 6) [30], HMIS coarsening with one level of aggressive coarsening (*hypre* type 10) [31], and a strength threshold of 0.05. These are similar parameters to the “optimized” parameters chosen for PDT transport runs in [32], with the important modification of using symmetric ℓ^1 hybrid Gauss-Seidel relaxation. In transport simulations, it is often the case that the spatial problem size per processor is relatively small, and ℓ^1 -relaxation can be faster/more robust [29]. AMG is used as a preconditioner for GMRES, which is solved to 10^{-4} relative residual tolerance.

Spatial linear transport equations are discretized using an upwind DG finite element method, constructed using the MFEM finite element library [33], and an S_N discretization is used in angle. As discussed in Section II, the angular flux vectors are eliminated from the system and only the scalar flux is stored and iterated on. Iterations are accelerated using fGMRES [34], an important choice when using AMG-preconditioned Krylov methods to solve the DSA matrix, as if the residual is not converged to very small tolerances, each iteration is actually a different preconditioner. It has been noted in multiple papers, originally in [5, 26], that Krylov acceleration is important for heterogeneous domains. The same is true for the new heterogeneous DSA algorithm proposed here, and we do not present unaccelerated (fixed-point) results. The code does not have a traditional parallel sweeping implementation, but angular flux problems are solved using the nonsymmetric AMG method based on approximate ideal restriction (AIR) [35, 36] in the *hypre* library [7].

IV.A. The crooked pipe problem

The first problem we consider is the so-called crooked-pipe problem, originally introduced in [17] and discussed as a benchmark for DSA in [18]. This is a steady state test problem for thermal radiative transport with a single energy group, and purely isotropic scattering throughout the domain. The domain is surrounded by vacuum, has a uniform isotropic radiation field, and has an inward isotropic source 10^4 times stronger than the radiation field. In [18], the problem is introduced with two scattering cross sections. Here we modify the domain to have five regions, shown in Figure 1, to allow for a larger variety of heterogeneities. Scattering cross section $\sigma_s(\mathbf{x})$ is defined to be piecewise constant over the subdomains shown in Figure 1, and total cross section is then defined as $\sigma_t(\mathbf{x}) = \sigma_s(\mathbf{x}) + 1/cdt$, where c is the speed of light and dt the time step of the transport solution. We use an S_8 angular discretization with 40 angles in the quadrature set (using the symmetry in 2D), and a 2nd-order DG finite element discretization of the linear spatial transport equation for each angle, unless otherwise noted.

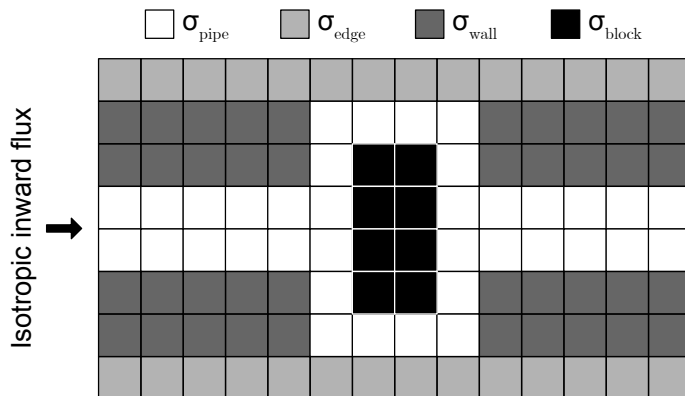


Fig. 1. A modification of the crooked pipe problem proposed in [18], here allowing for $\sigma_s(\mathbf{x})$ to have four different regions, denoted by varying shades from white to black.

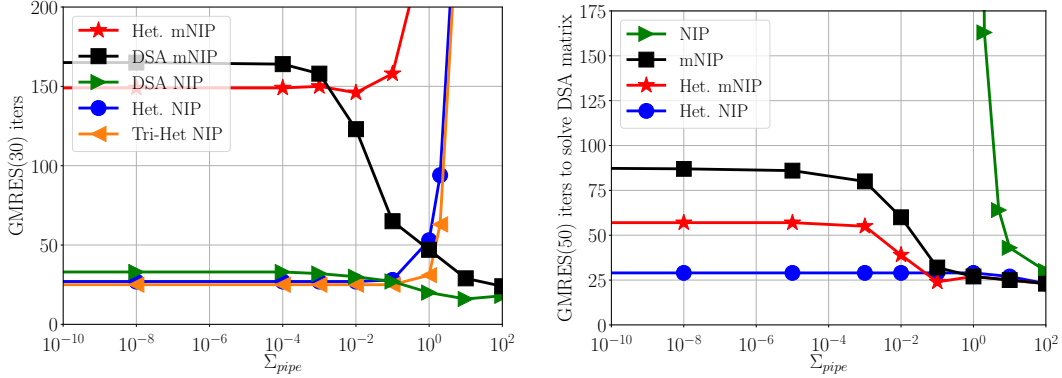
IV.A.1. Two cross sections

To start, we consider only two cross sections [17], one for the pipe (consistent with Figure 1) and one for the wall, consisting of everything outside of the pipe (wall, edge, and block as denoted in Figure 1). Consider the parameters used in [18],

$$\sigma_{\text{pipe}^c} = 200, \quad \sigma_{\text{pipe}} = 0.2, \quad cdt = 1000,$$

where $\sigma_{\text{pipe}^c} := \sigma_{\text{wall}} \cup \sigma_{\text{edge}} \cup \sigma_{\text{block}}$ is all regions outside of the pipe. Because these are only moderately heterogeneous coefficients, we instead fix $\sigma_{\text{pipe}^c} = 200$ and $cdt = 1000$ as above, then scale σ_{pipe} from zero to 100, to test a wide range of heterogeneities. Numerical tests compare the newly developed heterogeneous DSA with full DSA, using NIP and mNIP DG diffusion discretizations (see Section III.A).

We start by applying heterogeneous DSA only to σ_{pipe^c} (that is, outside of the pipe), even for $\sigma_{\text{pipe}} \geq 1$, in order to determine what values of σ require DSA for good convergence. Figure 2(a) shows the number of GMRES iterations to converge transport iterations to a relative residual tolerance of 10^{-12} (with DSA preconditioning applied directly using SuperLU [37]), and Figure 2(b) shows the number of AMG iterations to solve a representative DSA matrix to 10^{-12} relative residual. There are a number of observations to note from Figure 2:



(a) Comparison of GMRES iterations to 10^{-12} relative residual tolerance for various DSA and heterogeneous DSA preconditioners as a function of σ_{pipe} . DSA matrices are inverted directly.

(b) Total number of GMRES iterations, preconditioned by AMG, to solve the DSA matrix to a relative residual tolerance of 10^{-12} , for a single transport iteration.

Fig. 2. Results related to DSA preconditioners applied to the crooked pipe problem with $\sigma_{\text{pipe}^c} = 200$ and $cdt = 1000$, where heterogeneous DSA is only applied outside of the pipe. Note, results in Figures 2(a) and 2(b) are independent, separately demonstrating convergence of transport iterations and AMG.

- Full DSA with NIP is robust across the entire range of σ_{pipe} (green right-pointing triangles, Figure 2(a)), however, it is very difficult to solve for $\sigma_{\text{pipe}} \approx 1$ (green right-pointing triangles, Figure 2(b)), and we have tried many different variations of AMG and AMG-like techniques.
- Full DSA with mNIP is solvable with AMG (black squares, Figure 2(b)) and provides acceptable convergence of the transport iteration (black squares, Figure 2(a)), although mNIP requires about $5 \times$ more iterations than NIP.
- Heterogeneous DSA is applied *only outside of the pipe* for these tests, even when the pipe is moderately thick. As expected, convergence of heterogeneous DSA deteriorates rapidly when σ_{pipe} is not thin, as such regimes are known to require preconditioning. In practice, there is a switch so that DSA can be applied to all regions such that $\sigma_s(\mathbf{x}) \geq \eta$ for some tolerance η . If $\sigma_{\text{pipe}} > \eta$ for all \mathbf{x} , heterogeneous DSA breaks down to traditional DSA. Figure 2 suggests a tolerance of $\eta \approx 1.0$ to minimize the total number of iterations, while ensuring het-NIP DSA is solvable with AMG.

- For $\sigma_{\text{pipe}} < 0.1$, heterogeneous DSA with NIP or mNIP can provide up to a 25% reduction in total iterations from traditional DSA with NIP, and heterogeneous DSA with NIP provides up to a $5\times$ reduction of iterations compared to DSA with mNIP. Moreover, AMG solvers are robust when applied to heterogeneous DSA, taking between 23–55 iterations to obtain 12 digits of accuracy (blue circles and red stars, Figure 2(b)).
- Triangular heterogeneous DSA (Tri-Het. DSA) only offers a reduction in iteration count over diagonal heterogeneous DSA for a very small range of σ_{pipe} . For $\sigma_{\text{pipe}} \leq 0.1$, convergence is virtually identical. Because each iteration with the triangular preconditioning costs roughly twice as much as the diagonal preconditioning, it seems unlikely the triangular will be a better choice in practice, consistent with the discussion in Section II.C.

Based on these results, let the tolerance $\eta = 1$ moving forward. The following sections consider harder problems using full DSA and heterogeneous DSA with NIP and mNIP, now considering the modified σ -coefficients introduced in Section III.B for heterogeneous DSA for improved AMG performance.

IV.A.2. Multiple cross sections

Above, we took a benchmark problem and demonstrated the robustness and benefits of heterogeneous DSA. In this section, we take the same problem but use the full five regions of cross section indicated in Figure 1 to allow for a wider variety of heterogeneities and (hypothetically) more difficult problems. Table I provides five different sets of scattering cross sections, $\sigma_s(\mathbf{x})$, in the five subregions in Figure 1. Letting $\eta = 1$ distinguish between thick and thin regions, the percentage of the domain for each are also given.

Problem #	Parameters				Thin/thick	
	σ_{pipe}	σ_{wall}	σ_{edge}	σ_{block}	% Thin	% Thick
#1	1e-3	500	1e-4	100	55%	45%
#2	0.1	200	200	5	32%	68%
#3	1e-4	10	500	0.1	39%	61%
#4	1e-6	0.1	100	1000	68%	32%
#5	1e-4	10	500	100	32%	68%

TABLE I
Coefficients $\sigma_s(\mathbf{x})$ for five test problems.

Results using 32 cores and $\approx 2500 - 5000$ DOFs/core are shown in Table II. Tests are run for $cdt = 1, 1000$, and 10^8 , as well as the limiting case of zero absorption, $\sigma_a = 0$, and for 2nd- and 4th-order finite elements. All DSA matrices are inverted directly using SuperLU [37] in order to compare the preconditioning of S_N transport, independent of the solvability of the DSA matrix.

Note that the heterogeneous DSA method with NIP is as good or better than standard DSA in almost all cases. For some problems, heterogeneous DSA takes $5 - 6\times$ less iterations (see rows 14/15 and 19) than full DSA, or converges when full DSA with NIP does not (see rows 20 and 25). Results in Table II also provide important insight on the imposed σ_t boundary conditions for heterogeneous problems. Iteration counts for het-NIP and het-NIP(1) are almost identical, while mNIP(1) actually yields better convergence than mNIP, both of which are robust, although neither as effective as NIP. This is important because AMG performs significantly better on mNIP(1) and NIP(1) matrices than mNIP and NIP, respectively, so results in Table II suggest that such modified σ coefficients provide effective preconditioning, while making the associated linear solve easier.

Perhaps the most surprising result is that het-NIP_t performs identically to het-NIP and het-NIP(1) in all cases, except for problem #1 with $cdt \gg 1$, where it does not converge. This indicates that, for this problem, representing interface effects on boundary elements of

	Parameters			Full DSA		Heterogeneous DSA				
	Pr #	cdt	order	NIP	mNIP	NIP	NIP(1)	NIP _b	mNIP	mNIP(1)
1	#1	1	2	19	56	15	15	15	58	58
2	#2	1	2	18	41	15	15	15	47	47
3	#3	1	2	16	41	13	13	13	45	45
4	#4	1	2	19	58	15	15	15	59	59
5	#5	1	2	20	44	15	15	15	49	49
6	#1	10^3	2	31	120	25	23	DNC	124	109
7	#2	10^3	2	25	61	25	25	25	140	123
8	#3	10^3	2	23	96	20	20	20	96	82
9	#4	10^3	2	26	132	22	22	22	137	101
10	#5	10^3	2	102	143	25	25	25	133	136
11	#1	10^8	2	34	123	25	24	DNC	124	109
12	#2	10^8	2	25	64	25	25	25	141	124
13	#3	10^8	2	28	98	21	21	21	97	82
14	#4	10^8	2	116	134	22	22	22	138	102
15	#5	10^8	2	134	147	25	25	25	142	139
16	#1	$\sigma_a = 0$	2	34	153	25	24	DNC	124	109
17	#2	$\sigma_a = 0$	2	25	94	25	25	25	141	124
18	#3	$\sigma_a = 0$	2	24	128	21	21	21	97	82
19	#4	$\sigma_a = 0$	2	119	164	22	22	22	138	102
20	#5	$\sigma_a = 0$	2	DNC	177	25	25	25	142	139
21	#1	$\sigma_a = 0$	4	42	79	25	25	DNC	78	79
22	#2	$\sigma_a = 0$	4	59	40	36	37	39	57	56
23	#3	$\sigma_a = 0$	4	59	57	21	21	21	57	56
24	#4	$\sigma_a = 0$	4	59	73	22	22	22	73	71
25	#5	$\sigma_a = 0$	4	DNC	70	27	27	27	70	67

TABLE II

DSA-preconditioned GMRES(30) iterations to 10^{-12} relative residual for Problems #1 – #5, with an S_8 angular discretization and 2nd- or 4th-order DG spatial discretization (DNC denotes did not converge in 500 iterations). See Section III.A for details on NIP, NIP(1), NIP_b, and mNIP.

the thick subdomain in the DSA discretization is fundamental to convergence. The inclusion does not need to be significant, as NIP(1) simply treats thin neighbor elements as $\sigma_t = 1$ and converges rapidly (and nearly identical results can be obtained for NIP(10)), but extending $\sigma_t = 100$ and 500 to neighboring elements of the thick subdomain (see Table I) results in no convergence. We do not have a rigorous explanation for why NIP_b fails on this problem, but by counter-example it rules out the NIP_b method as a parameter-free and easy-to-solve option.

Next we consider a refined spatial mesh, with an S_8 angular discretization and 2nd-order DG finite elements ($\approx 1M$ spatial DOFs), and look at convergence of DSA preconditioned with NIP, mNIP, het-NIP(1), and het-mNIP(1). All simulations are run on 256 cores, and DSA solves are performed using a maximum of 250 AMG iterations. In Table III, we see that full DSA with NIP does not converge for $cdt \gg 1$, largely because 250 AMG iterations provide a very poor approximation to the diffusion inverse. On the refined mesh, mNIP iterations to convergence actually decrease (compared with Table II) and each iteration only requires a modest number of AMG iterations. However, het-mNIP(1) provides comparable convergence for the transport iterations, while the heterogeneous DSA solves require a fraction of the number of AMG iterations of full DSA ($20\times$ less for Problem #1 and $cdt = 10^8$). Heterogeneous

Parameters		DSA NIP		DSA mNIP		Het. DSA NIP(1)		Het. DSA mNIP(1)	
Pr #	<i>cdt</i>	Iters.	AMG it.	Iters.	AMG it.	Iters.	AMG it.	Iters.	AMG it.
#1	1	35	DNC	39	14	15	48	40	11
#2	1	27	DNC	23	8	17	43	26	5
#3	1	34	DNC	29	10	13	32	32	7
#4	1	38	DNC	42	10	13	8	41	6
#5	1	37	DNC	30	10	14	32	34	7
#1	10^3	DNC	DNC	73	99	25	38	73	6
#2	10^3	DNC	DNC	40	13	29	119	55	7
#3	10^3	DNC	DNC	55	33	22	37	54	8
#4	10^3	DNC	DNC	71	26	23	11	70	6
#5	10^3	DNC	DNC	78	34	27	37	81	8
#1	10^8	DNC	DNC	71	145	25	42	73	6
#2	10^8	DNC	DNC	40	12	29	119	54	7
#3	10^8	DNC	DNC	55	42	22	37	54	9
#4	10^8	DNC	DNC	73	43	22	11	70	7
#5	10^8	DNC	DNC	75	41	27	37	83	8

TABLE III

DSA-preconditioned *f*GMRES(30) iterations to 10^{-12} relative residual (“Iters.”), and AMG-preconditioned GMRES iterations to apply a single DSA preconditioning to 10^{-4} relative-residual (“AMG It.”).

DSA with het-NIP(1) provides a $2 - 3\times$ reduction in total transport iterations, for a typically comparable number of AMG iterations. Overall, the heterogeneous DSA variations can offer a significant reduction in time to solution, either reducing the total number of iterations, reducing the number of necessary AMG iterations, or both.

IV.B. Hohraum

The second problem we consider represents a realistic setting of the hohlraum chamber with a fuel capsule. This design is used in the indirect-drive approach of inertial confinement fusion (ICF). Radiation transport plays a fundamental role in the indirect-drive scenario, where the gold wall of the hohlraum, heated by lasers to a high temperature, radiates x-rays that propagate through a low density Helium fill. This causes a compression of the fuel capsule as the photons are absorbed on its surface. The capsule is filled with hydrogen, contained inside a thin layer of plastic (CH) on its surface, with a small hole on the right simulating a filling tube. The cross section and emissivity of a material is strongly dependent on its composition and temperature, making x-ray radiation transport a highly non-linear process.

This can be represented by a time-dependent thermal radiative transfer problem modeled by a transport equation with a “pseudo-scattering” term [38, 39], σ_{ps} , and a corresponding source of gray-body approximation, q_{ps} :

$$\sigma_{ps} = \frac{\sigma^2 16\pi a c T^3}{\frac{C_v}{\Delta t} + 16\pi\sigma a c T^3}, \quad (22)$$

$$q_{ps} = \sigma_a a c T^4 - \frac{\sigma^2 16\pi a^2 c^2 T^7}{\frac{C_v}{\Delta t} + 16\pi\sigma a c T^3}, \quad (23)$$

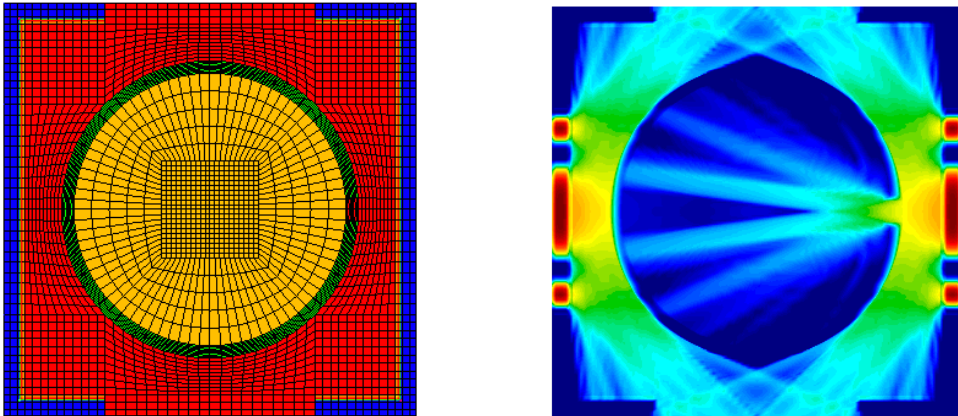
both as a function of coefficient σ . Here, T is the plasma temperature, C_v the heat capacity, $c = 2.9979 \times 10^4$, $a = 137.199$ the radiation constant, and we use a very long time step $\Delta t = 10^{-3}\mu\text{s}$, corresponding to $\approx 10\%$ of the duration of a common ICF simulation. The unit system

of National Ignition Facility is used [40]. The hohlraum problem introduces four different materials: gold (blue), helium (red), CH (green), and hydrogen (yellow), each with a different cross section and heat capacity as shown in Figure 3(a), and with corresponding σ and C_v values given in Table IV.

	hohlraum gold wall	helium fill	capsule CH layer	capsule hydrogen fuel
σ	10^3	10^{-3}	10^2	1
C_v	10^5	10^{-2}	10^3	1

TABLE IV
Opacities, $\sigma_a(\mathbf{x})$, and heat capacities, $C_v(\mathbf{x})$, for given materials.

Here we consider a steady state test of a single time step, modeled by (2) with a single energy group, and purely isotropic scattering throughout the domain. In the notation of (2), we have $\sigma_s(\mathbf{x}) = \sigma_{ps}(\mathbf{x})$ and $\sigma_t(\mathbf{x}) = \sigma(\mathbf{x})$, with the radiation source as $q_d(\mathbf{x}) = q_{ps}(\mathbf{x})$. The domain is surrounded by vacuum, has an initially uniform temperature $T = 10^{-3}$ keV, and the source q_{ps} on the hohlraum gold wall corresponds to $T = 0.4$ keV. The solution of the scalar flux radiation field produced by a laser-heated gold wall is shown in Figure 3(b). In large-scale problems the “pseudo scattering” equation is solved iteratively, and standard iterative methods converge very slowly when either the time step or σ is large. Extreme heterogeneities are encountered in such cases, in particular on the gold-helium and CH-helium material interfaces.



(a) Hohlraum mesh, with materials represented as colors: gold \leftrightarrow blue, helium \leftrightarrow red, CH \leftrightarrow green, and hydrogen \leftrightarrow yellow (left-to-right: blue, red, green, yellow, green, red, blue). (b) Scalar flux solution (S_{18}) due to radiation source from the laser-heated gold wall (red regions \sim laser heating).

Fig. 3. Indirect-drive ICF approach using a gold cylindrical chamber (hohlraum) filled with helium and a fuel capsule placed in the middle.

Table V shows results for DSA and het-DSA preconditioning of a 4th-order DG discretization in space, and S_4 , S_8 , and S_{12} angular discretizations. Simulations are run on 16, 64, and 256 cores, corresponding to the three levels of refinement shown, with ≈ 5000 spatial DOFs/core. Performance of AMG on the hohlraum problem is particularly poor for full DSA. Results for full DSA with NIP are not shown in Table III because AMG iterations make no significant reduction in residual for the DSA solve and, thus, the larger transport iterations do not converge. AMG is also unable to solve the full DSA with mNIP matrices (1,000 AMG-preconditioned GMRES iterations reduced the residual less than two orders of magnitude), but apparently enough preconditioning is achieved in 250 iterations for the larger transport iterations to achieve reasonable convergence. However, we would not consider this a robust method, as results for full DSA with NIP here and in Table III indicate that if the AMG

iterations are ineffective, the preconditioning may also be ineffective, and the transport iterations may not converge. Moreover, it is likely AMG convergence will continue to degrade as the spatial problem is further refined, which may eventually prevent convergence of the larger transport iterations. Note, we also tried multiple scaling constants for mNIP and saw no notable improvement in AMG convergence.

S_N	DOFs	DSA mNIP		Het. DSA NIP(10)		Het. DSA mNIP(10)	
		Iters.	AMG it.	Iters.	AMG it.	Iters.	AMG it.
4	78,900	52	DNC	28	27	29	10
4	315,600	40	DNC	27	38	27	14
4	1,262,400	28	DNC	22	582	22	12
8	78,900	52	DNC	29	26	29	10
8	315,600	40	DNC	27	43	28	14
8	1,262,400	29	DNC	22	674	23	12
12	78,900	52	DNC	28	26	28	10
12	315,600	39	DNC	27	43	28	14
12	1,262,400	29	DNC	20	685	23	12

TABLE V

DSA-preconditioned fGMRES iterations to 10^{-12} relative residual, and AMG-preconditioned GMRES iterations to 10^{-4} relative residual tolerance (with a maximum 250 AMG iterations), for the hohlraum problem.

In contrast, heterogeneous DSA proves to be fast and robust with NIP and mNIP. Here we use het-NIP(10), which makes the het-NIP AMG solves converge faster than het-NIP(1), and het-mNIP(10) for a fair comparison (note, nearly identical iteration counts for AMG and the transport solution can be obtained with het-mNIP(1)). Heterogeneous DSA converges in fewer iterations than full DSA for all tested problem sizes and S_N orders, in all cases reducing total iteration count by 20 – 45%. Moreover, AMG proves effective as a solver for het-NIP(10) and het-mNIP(10), with het-mNIP requiring only 10–15 AMG iterations to reduce the residual four orders of magnitude. This highlights how interesting the dynamics of the problem and preconditioning can be: without DSA preconditioning, source iteration on this problem converges extremely slow. Preconditioning a very small subdomain (only 3.3% of the mesh elements!) with 10–15 AMG iterations results in rapid convergence, independent of spatial mesh refinement or S_N order.

V. CONCLUSIONS

This paper introduces a new DSA-like technique to precondition transport iteration in highly heterogeneous domains, which is trivially compatible with voids. The preconditioning is based on a linear algebraic analysis rather than the underlying physics, but proves to be at least as fast as standard “full” DSA on all problems we tested, and reduces the iteration count by 5 – 6× on some examples. Moreover, even for robust DSA discretizations based on integrating angular moments, the resulting linear systems are solvable using AMG and the *hypre* library. Although the new method does not fully address the problem of discontinuous DSA matrices being difficult to invert in parallel using, e.g., AMG (for example, see AMG iters. for heterogeneous NIP in Table V) the matrices resulting from the heterogeneous algorithm are much more tractable to invert than the global DSA matrices on highly heterogeneous domains.

Even with optimized AMG parameters and a state-of-the-art parallel AMG library, the application of DSA can take a remarkably large portion of the solve phase for S_N transport, as high as 60% with a small number of mesh elements per core [32]. For difficult problems like the hohlraum discussed in Section IV.B, AMG simply does not converge, and it is unclear if the preconditioned transport iterations will converge. In addition to making the DSA solves

tractable, only having to solve a DSA discretization on the moderately thick to thick subdomains can also significantly reduce the percentage of time the DSA solves take. The hohlraum problem studied in Section IV.B only requires DSA preconditioning on $\approx 3\%$ of the mesh elements for rapid convergence. Finally, the proposed approach is relatively non-intrusive and easy to add to existing high-performance transport codes.

Numerical results in Section IV indicate rather different behavior on different heterogeneous configurations of σ_t , in terms of DSA preconditioning and AMG convergence. This can be seen as the appropriate choice of boundary conditions on the thick subdomain, but analyzing this problem is nontrivial as it is based on an approximation to a sum of Schur complement inverses (15). A unified framework for DSA preconditioning, including the heterogeneous approach developed here as well as a better understanding of how discretization properties and parameters affect both DSA preconditioning and the performance of multigrid-like solvers, remains an outstanding issue and long-term objective.

ACKNOWLEDGMENTS

This material is based upon work supported by the Department of Energy, National Nuclear Security Administration, under Award Number DE-NA0002376. This work was performed under the auspices of the U.S. Department of Energy by Lawrence Livermore National Laboratory under contract DE-AC52-07NA27344 (LLNL-JRNL-802400). Disclaimer: This document was prepared as an account of work sponsored by an agency of the United States government. Neither the United States government nor Lawrence Livermore National Security, LLC, nor any of their employees makes any warranty, expressed or implied, or assumes any legal liability or responsibility for the accuracy, completeness, or usefulness of any information, apparatus, product, or process disclosed, or represents that its use would not infringe privately owned rights. Reference herein to any specific commercial product, process, or service by trade name, trademark, manufacturer, or otherwise does not necessarily constitute or imply its endorsement, recommendation, or favoring by the United States government or Lawrence Livermore National Security, LLC. The views and opinions of authors expressed herein do not necessarily state or reflect those of the United States government or Lawrence Livermore National Security, LLC, and shall not be used for advertising or product endorsement purposes.

REFERENCES

- [1] HJ Kopp. Synthetic method solution of the transport equation. *Nuclear Science and Engineering*, 17(1):65–74, 1963.
- [2] VI Lebedev. The iterative kp method for the kinetic equation. In *Proc. Conf on Mathematical Methods for Solution of Nuclear Physics Problems*, pages 17–20, 1964.
- [3] R E Alcouffe. Diffusion Synthetic Acceleration Methods for the Diamond-Differenced Discrete-Ordinates Equations. *Nuclear science and engineering*, 64:344–355, 1977.
- [4] E W Larsen. Unconditionally Stable Diffusion-Synthetic Acceleration Methods for the Slab Geometry Discrete Ordinates Equations Part 1: Theory. *Nuclear science and engineering*, 82(1):47–63, 1982.
- [5] J S Warsa, T A Wareing, and J E Morel. Krylov Iterative Methods and the Degraded Effectiveness of Diffusion Synthetic Acceleration for Multidimensional S_N Calculations in Problems with Material Discontinuities. *Nuclear science and engineering*, 147(3):218–248, July 2004.
- [6] T. S. Haut, B. S. Southworth, V. Z. Tomov, and P. G. Maginot. A DSA Preconditioner for the S_N Transport Equations on High-order Curved Meshes. *SIAM J. Sci. Comput.* (in review), Oct. 2018.

- [7] R D Falgout and U M Yang. hypre: A library of high performance preconditioners. *European Conference on Parallel Processing*, 2331 LNCS(PART 3):632–641, 2002.
- [8] J S Warsa, M Benzi, T A Wareing, and J E Morel. Two-level preconditioning of a discontinuous Galerkin method for radiation diffusion. In *Numerical Mathematics and Advanced Applications*, pages 967–977. Springer, Springer Italia, Milan, 2003.
- [9] B O’Malley, J Kópházi, R P Smedley-Stevenson, and M D Eaton. Hybrid Multi-level solvers for discontinuous Galerkin finite element discrete ordinate diffusion synthetic acceleration of radiation transport algorithms. *Annals of Nuclear Energy*, 102:134–147, April 2017.
- [10] L N Olson and J B Schroder. Smoothed aggregation multigrid solvers for high-order discontinuous Galerkin methods for elliptic problems. *Journal of Computational Physics*, 230(1):6959–6976, August 2011.
- [11] Peter Bastian, Markus Blatt, and Robert Scheichl. Algebraic multigrid for discontinuous Galerkin discretizations of heterogeneous elliptic problems. *Numerical Linear Algebra with Applications*, 19(2):367–388, February 2012.
- [12] Paola F Antonietti, Marco Sarti, Marco Verani, and L T Zikatanov. A Uniform Additive Schwarz Preconditioner for High-Order Discontinuous Galerkin Approximations of Elliptic Problems. *Journal of Scientific Computing*, 70(2):608–630, August 2016.
- [13] Y Wang, H Zhang, and Richard C Martineau. Diffusion Acceleration Schemes for Self-Adjoint Angular Flux Formulation with a Void Treatment. *Nuclear science and engineering*, 176(2):201–225, March 2017.
- [14] Hans R Hammer, J E Morel, and Y Wang. Nonlinear Diffusion Acceleration of the Least-Squares Transport Equation in Geometries with Voids. *Nuclear science and engineering*, 193(5):453–480, January 2019.
- [15] Shuai Ye, Hengbin An, and Xinhai Xu. A local character based method for solving linear systems of radiation diffusion problems. *Journal of Computational Physics*, page 109218, 2020.
- [16] Y Wang and J C Ragusa. Diffusion Synthetic Acceleration for High-Order Discontinuous Finite Element S-N Transport Schemes and Application to Locally Refined Unstructured Meshes. *Nuclear science and engineering*, 166(2):145–166, October 2010.
- [17] NA Gentile. Implicit monte carlo diffusion – an acceleration method for monte carlo time-dependent radiative transfer simulations. *Journal of Computational Physics*, 172(2):543–571, 2001.
- [18] R P Smedley-Stevenson, A W Hagues, and J Kópházi. A Benchmark for Assessing the Effectiveness of Diffusion Synthetic Acceleration Schemes. In *Joint International Conference on Mathematics and Computation MC, Supercomputing in Nuclear Applications SNA and the Monte Carlo MC Method*, pages 1–16. American Nuclear Society, February 2015.
- [19] V Faber and T A Manteuffel. A look at transport theory from the point of view of linear algebra. In *Transport theory, invariant imbedding, and integral equations (Santa Fe, NM)*, pages 37–61. Dekker, New York, 1989.
- [20] B. S. Southworth, A. A. Sivas, and S. Rhebergen. On fixed-point, krylov, and 2×2 block preconditioners. *arXiv preprint arXiv:1911.02664*, 2020.
- [21] JS Warsa, K Thompson, and JE Morel. Improving the efficiency of simple parallel S_N algorithms with krylov iterative methods. *TRANSACTIONS-AMERICAN NUCLEAR SOCIETY*, pages 449–451, 2003.

- [22] T. S. Haut, P. G. Maginot, V. Z. Tomov, B. S. Southworth, T. A. Brunner, and T. S. Bailey. An Efficient Sweep-based Solver for the S_N Equations on High-order Meshes. *Nuclear Science and Engineering*, pages 1–14, Jan. 2019.
- [23] Yaqi Wang. *Adaptive mesh refinement solution techniques for the multigroup S_N transport equation using a higher-order discontinuous finite element method*. Texas A&M University, 2009.
- [24] Gene H Golub and Charles F Van Loan. *Matrix Computations*, volume 4. JHU Press, 2013.
- [25] B. S. Southworth and S. S. Olivier. A note on 2×2 block-diagonal preconditioning. *arXiv preprint arxiv:2001.00711*, 2019.
- [26] A Gupta and R S Modak. On the use of the conjugate gradient method for the solution of the neutron transport equation. *Annals of Nuclear Energy*, 29(16):1933–1951, November 2002.
- [27] B Chang. The conjugate gradient method solves the neutron transport equation h-optimally. *Numerical Linear Algebra with Applications*, 14(10):751–769, December 2007.
- [28] J S Warsa, T A Wareing, and J E Morel. Fully consistent diffusion synthetic acceleration of linear discontinuous S(N) transport discretizations on unstructured tetrahedral meshes. *Nuclear science and engineering*, 141(3):236–251, July 2002.
- [29] A H Baker, R D Falgout, T V Kolev, and U M Yang. Multigrid smoothers for ultraparallel computing. *SIAM Journal on Scientific Computing*, 33(5):2864–2887, 2011.
- [30] H De Sterck, R D Falgout, J W Nolting, and U M Yang. Distance-two interpolation for parallel algebraic multigrid. *Numerical Linear Algebra with Applications*, 15(2-3):115–139, 2008.
- [31] H De Sterck, U M Yang, and J J Heys. Reducing Complexity in Parallel Algebraic Multigrid Preconditioners. *SIAM Journal on Matrix Analysis and Applications*, 27(4):1019–1039, January 2006.
- [32] Milan Hanus. Weak scaling of dsa preconditioning of transport sweeps using hypre. *arXiv preprint arXiv:1911.04624*, 2019.
- [33] V. A. Dobrev, T. V. Kolev, et al. MFEM: Modular finite element methods. <http://mfem.org>, 2018.
- [34] Y Saad. A Flexible Inner-Outer Preconditioned Gmres Algorithm. *SIAM Journal on Scientific Computing*, 14(2):461–469, March 1993.
- [35] T A Manteuffel, J W Ruge, and B S Southworth. Nonsymmetric algebraic multigrid based on local approximate ideal restriction (ℓ AIR). *SIAM Journal on Scientific Computing*, 40(6):A4105–A4130, Dec. 2018.
- [36] T. A. Manteuffel, S. Munzenmaier, J. Ruge, and B. S. Southworth. Nonsymmetric reduction-based algebraic multigrid. *SIAM J. Sci. Comput.*, 41(5):S242–S268, 2019.
- [37] Xiaoye S Li, James W Demmel, John R Gilbert, Laura Grigori, Meiyue Shao, and Ichitaro Yamazaki. Superlu users’ guide. *Lawrence Berkeley National Laboratory*, 1999.
- [38] J A Fleck and Cummings J D. An implicit monte carlo scheme for calculating time and frequency dependent nonlinear radiation transport. *Journal of Computational Physics*, 8(3):313, 1971.
- [39] E W Larsen. A grey transport acceleration method for time-dependent radiative transfer problems. *Journal of Computational Physics*, 78:459, 1988.

- [40] M.M. Marinak, G.D. Kerbel, Joseph Koning, Mehul Patel, S.M. Sepke, P. Brown, B. Chang, R.J. Procassini, and S. Veitzer. Advances in hydra and its application to simulations of inertial confinement fusion targets. *EPJ Web of Conferences*, 59, 01 2008.